JOURNAL OF SPACECRAFT AND ROCKETS
Vol. 46, No. 6, November–December 2009

Empirical and Computational Performance Prediction for Monopropellant Hydrazine Thruster Employed for Satellite

Dong In Han*
Korea Advanced Institute of Science and Technology, Daejeon 305-701, Republic of Korea
Cho Young Han†
Korea Aerospace Research Institute, Daejeon 305-333, Republic of Korea
and
Hyun Dong Shin‡
Korea Advanced Institute of Science and Technology, Daejeon, 305-701, Republic of Korea

DOI: 10.2514/1.43739

A ground hot-fire test and numerical simulations were conducted to analyze the high-temperature gas flow in a monopropellant hydrazine thruster used for the reaction control of small satellites. A 5 N grade thruster was used for these tests and simulations. The ground hot-fire test results show the basic characteristics of a hydrazine thruster and were used as verification criteria for the numerical analysis. It was found that the fraction of ammonia dissociation is an essential variable for determining the thruster performance based on a one-dimensional isentropic analysis. A relatively simple relation between the catalyst bed temperature and the fraction of ammonia dissociation adopted in the simulation showed that it reduces the analysis error from an arbitrary assumption of the fraction of ammonia dissociation without solving the complicated hydrazine catalytic reaction. The thruster performance was effectively predicted by numerical analysis, which includes the effect of fraction of ammonia dissociation. The significant features of the analysis program are that solving the complicated hydrazine decomposition process can be avoided and that two-dimensional flowfield information in the thruster can be provided covering a wide range of propellant inlet pressures from 3.45 to 24.14 bar.

Nomenclature

I_{sp}	=	specific impulse
M	=	Mach number
$\dot{m}_p$	=	propellant mass flow rate
Pc	=	decomposition chamber pressure
P_i	=	propellant inlet pressure
Tc	=	decomposition chamber temperature
u, v	=	velocity in the x and y directions, respectively
ρ	=	density
χ	=	fraction of ammonia dissociation

I. Introduction

REACTION control thrusters are widely used in spacecraft chemical propulsion systems for various missions. Monopropellant hydrazine thrusters are used extensively as a reaction control thruster due to their unlimited restart capability and high reliability [1–3]. A low-Earth-orbit satellite requires impulse applications for various purposes, such as the injection of the satellite into mission orbit, the drag force compensation, the acceleration and deceleration of the satellite along its moving axis, and the satellite's three axis attitude controls. Monopropellant hydrazine thrusters are generally employed to provide the thrust required for satellites.

There is an increasing demand to develop monopropellant thrusters with various capabilities as satellite missions become more complicated. During the last several decades, costly and inherently risky testing has been performed to validate the performance and reliability of monopropellant thrusters. However, to reduce the thruster development time, cost, and risk, there is a demand to replace such tests with numerical simulations. Numerical simulation program development for the monopropellant thruster is aimed at efficient thruster development and design change management.

A monopropellant hydrazine thruster consists of an injector, catalyst bed, and nozzle. The liquid hydrazine in the propellant tank is injected into the catalyst bed through an injector. As the result of the decomposition of hydrazine, high-temperature gases are produced in the catalyst bed and then expelled through a converging–diverging nozzle, producing thrust.

The study of hydrazine catalytic reactions for satellite thruster applications started in 1949 at the California Institute of Technology's Jet Propulsion Laboratory (JPL) [4,5]. Kersten [6] and Shankar et al. [7] presented mathematical models of hydrazine catalytic decomposition with an iridium catalyst. These studies focused particularly on high-temperature gas generation by the hydrazine catalytic reaction in the catalyst bed. Hearn and Young [8] showed a numerical analysis relating to the performance of a satellite propulsion system with a hydrazine thruster. Performance of the propulsion system was evaluated based on a mathematical model using ordinary differential equations and empirical data. Two years later, Hearn [9] conducted a comparison analysis between flight data and ground test data. Subhash [10] presented a simple test model for predicting the performance of a hydrazine thruster as well.

Shankar et al. [11] acquired test data using a hydrazine thruster developed in India and compared the data with those of a theoretical one-dimensional isentropic model. A performance analysis revealed that their results were comparatively well predicted, despite being based on two primary assumptions: 1) the hydrazine catalytic

Received 11 February 2009; revision received 14 June 2009; accepted for publication 21 June 2009.

*Senior Researcher, Mechanical Engineering, 335 Gwahangno Guseong-Dong Yuseong-Gu; dihan@kari.re.kr.

†Senior Researcher, Satellite Thermal and Propulsion Department, Satellite Research and & Development Head Office, 45 Eoeun-Dong Yuseong-Gu; cyhan@kari.re.kr (Corresponding Author).

‡Professor, Mechanical Engineering, 335 Gwahangno Guseong-Dong Yuseong-Gu; hdshin@kaist.ac.kr.

reaction was limited within the catalyst bed, and 2) the chemical compositions caused by a hydrazine catalytic reaction for nozzle flow were in a frozen equilibrium condition [12,13]. However, these simulation results are valid for only one particular design condition.

Multidimensional numerical simulations and ground tests for predicting hydrazine thruster performance have also been conducted. Kushida et al. [14] carried out a test to determine the variation in thrust from different nozzle area ratios. Their test results were verified using two-dimensional kinetics, that is, a nozzle performance analysis program. The performance prediction and evaluation methods of JANNAF were used in their work. It was found that these methods can be applied to a small rocket thruster, which has a thick boundary layer at the nozzle exit. The JANNAF methods are widely used in the United States for the numerical analysis of rocket engine performance design. However, access to the JANNAF method is strictly limited for foreign researchers due to legal issues.

The objective of this study was to develop a numerical simulation program for analyzing, predicting, and evaluating the performance of a monopropellant hydrazine thruster. These numerical simulation results were verified by ground hot-fire test results. Instead of performing complicated mathematical modeling of the hydrazine decomposition in the catalyst bed, the input conditions of the chemical compositions for nozzle flow were obtained based on a simple mathematical correlation between the exit temperature of the catalyst bed and the fraction of ammonia dissociation. An axisymmetric two-dimensional Navier–Stokes solver was used for nozzle flow analysis.

Thruster performance analyses were performed according to various propellant inlet conditions, and their results were compared with those of the ground hot-fire test results. The numerical simulation has the advantage of being able to provide two-dimensional nozzle flow data, which are difficult to obtain from the ground hot-fire tests; it can also be used to assist in a design change of the hydrazine thruster.

This paper presents ground hot-fire test results and numerical analysis results using the Navier–Stokes solver with various inlet propellant pressure conditions simultaneously. It is assumed that the numerical program, which was developed based on the simple correlation formula, is useful for predicting hydrazine thruster performance in the case of a preliminary design phase, without the use of costly and risky hot-fire tests.

The satellite monopropellant hydrazine thruster used in the hot-fire test was a Korea Aerospace Research Institute (KARI) satellite thruster, and its nominal thrust is 4.5 N. Figure 1 shows a sectional view of the thruster. Hydrazine propellant is injected into the catalyst bed through a propellant valve, a feed tube, and an injector. The catalyst bed is composed of iridium coated alumina grains. A screen is installed between the injector and catalyst bed to prevent the outflow of catalyst particles from the catalyst bed and also to ensure that the propellant is injected evenly to the catalyst. The maximum steady-state thrust of the thruster at the beginning of life is 4.5 N at a propellant inlet pressure of 24.1 bar, and the minimum steady-state thrust at the end of life is 0.9 N at a propellant inlet pressure of 3.4 bar.

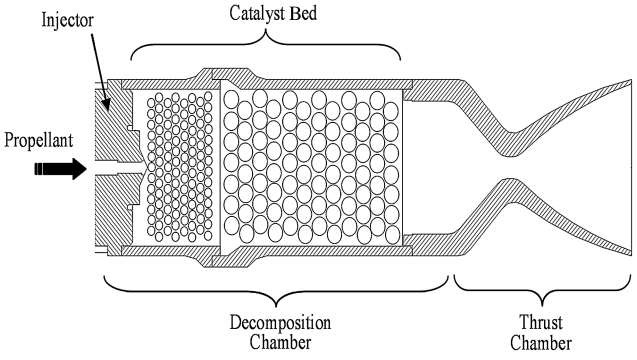

Fig. 1 Sectional view of monopropellant hydrazine thruster.

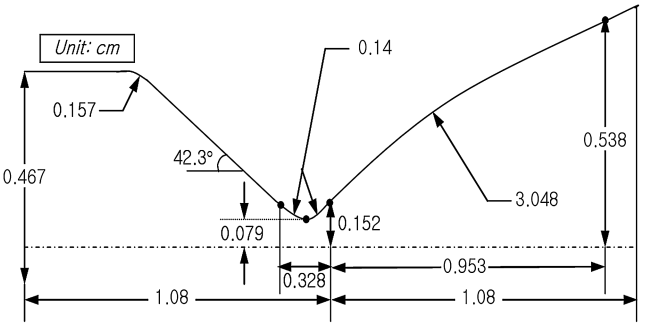

Fig. 2 Dimensions of monopropellant hydrazine thruster.

The steady-state specific impulse ranges from 202 to 221 s for a propellant inlet pressure range of 4.48–21.37 bar.

Figure 2 illustrates the dimensions of the thruster chamber. The radius of the nozzle exit is 5.63 mm, and that of the nozzle throat is 0.79 mm. The nozzle exit to nozzle throat area ratio is 50.8. Thrusters are classified by the bending angle between the centerline of the nozzle and the centerline of the thruster. Nozzles can be bent at an angle of 0, 30, and 90 deg to the centerline of the thruster. In practice, thrusters with a 30 deg bent nozzle are used for satellite applications. The thruster with a straight nozzle, however, is modeled in the numerical analysis for convenience of the simulation.

II. Ground Hot-Fire Test

A ground hot-fire test was conducted inside a vacuum chamber, which was depressurized to a pressure of 0.0103 bar to simulate an altitude of 30 km. Hydrazine monopropellant, which meets the MIL-PRF-26536D requirements, was used as the working fluid and was filtered by a 10 μm filter before injection into the catalyst bed.[§]

Figure 3a shows the mechanical connection used to join the thrust measurement rig and the thruster. The thrust measurement rig provides mechanical and thermal compensation with its self-correction capability under vacuum conditions. Figure 3b illustrates the thruster's glowing phenomenon during the hot-fire test. The temperature of the heated thruster exceeded 1200 K.

The raw test data before compensation were converted to vacuum thrust after vacuum correction, and the specific impulse, which accounts for the mass flow rate, was derived.

Table 1 summarizes the results of the ground hot-fire test. The temperature (T_C) and pressure (P_C) of the decomposition chamber, the steady-state thrust (SST), and the specific impulse (I_{sp}) were measured at various values of the propellant inlet pressure. Hydrazine propellant was injected into the catalyst bed, which had a temperature of 294 K, and the electrical pulse width signals were longer than 60 s to achieve the steady-state conditions. The steady-state thrust and specific impulse values shown in Table 1 are the values after vacuum correction.

Expressions for some of the data related to characteristics of the nozzle flow to the propellant inlet pressure were determined from the curve that fits the test data shown in Table 1, in which the inlet pressure, P_i, is measured in bars:

$$T_C[^\circ\mathrm{C}] = 0.017P_i^3 - 1.287P_i^2 + 33.293P_i + 604.936 \quad (1)$$

$$P_C[\mathrm{bar}] = 0.494P_i + 1.021 \quad (2)$$

$$\dot{m}_p[\mathrm{g/s}] = 7.434 \times 10^{-2}P_i + 0.213 \quad (3)$$

Equations (1–3) were used as the initial values for the simulation model and to verify the simulation results. The functions and measured data are shown in Fig. 4.

[§]MIL-PRF-26536D, Performance Specification Propellant, Hydrazine.

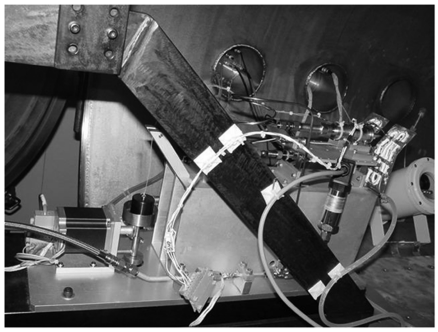

a) Thrust measurement rig

b) Glowing during steady-state firing

Fig. 3 Hot-fire test configuration.

III. Numerical Simulation of Internal Flow of Thruster

The subsonic velocity area and supersonic velocity area coexist inside a rocket engine thruster. Any algorithm for a numerical analysis of the thruster, therefore, covers both the compressible flow and the incompressible flow regimes. Solution algorithms for compressible flow may not be suitable for the low-speed regime because the eigenvalues of the system become stiff or the pressure term in the momentum equation becomes singular due to the Mach number. In addition, the solution may not converge or an incorrect solution may be deduced if a compressible flow solution algorithm is applied to a subsonic flow analysis, due to the character of the algorithm. Chen and Shuen [15] modified the equation to attain consistent convergence for any Mach number by adding a time preconditioning term to rescale the system eigenvalues and by decomposing the pressure variation into a constant reference pressure term and a gauge pressure term.

In this study, the time preconditioning method, the pressure term dividing method, and the second-order central difference method were applied to compressible flow equations. The simulation results were verified by the JPL nozzle test results [16].

A. Governing Equations

The governing equation, which was used to solve for flow inside a thruster, covers the entire range of speeds because the flow velocity of the thruster develops from subsonic to supersonic. The Navier–Stokes equation of two-dimensional, unsteady, compressible flow written in nonorthogonal coordinates can be expressed by the following numerical formula [17]:

$$\frac{\partial}{\partial \tau}\tilde{Q} + \frac{\partial}{\partial \xi}(\tilde{E} - \tilde{E}_v) + \frac{\partial}{\partial \eta}(\tilde{F} - \tilde{F}_v) = 0 \tag{4}$$

where τ is the time coordinate, and ξ and η are the spatial coordinates.

A compressible flow equation, such as Eq. (4), is not efficient for solving an incompressible, low-Mach-number flow because the pressure term increases as $1/M^2$ decreases compared with the convective term. Thus, a special modification of a compressible flow equation was required for the stable analysis of a flow in which the Mach number varies widely [15]. The pressure dividing method, the precondition method, and the pseudotime term adding method were incorporated into the governing equations to improve the convergence of a solution.

Table 1 Hot-fire test results

P_i, bar	P_C, bar	T_c, °C	SST, N	I_{sp}, s	$\dot{m}_p$, g/s
4.42	3.1	728	0.99	211.52	0.48
4.47	3.0	734	1.00	223.45	0.46
6.99	4.6	770	1.51	218.14	0.71
7.69	5.0	792	1.67	220.29	0.77
7.94	5.1	803	1.68	241.90	0.72
17.13	9.8	880	3.28	223.14	1.50
17.43	9.9	888	3.42	226.61	1.54
24.00	12.8	889	4.51	230.99	1.99
26.40	14.0	887	4.64	227.42	2.08
26.48	13.9	894	4.76	227.01	2.14

The preconditioned matrix,

$$\begin{bmatrix} 1/\beta & 0 & 0 & 0 & 0 & \cdots \\ u/\beta & \rho & 0 & 0 & 0 & \cdots \\ v/\beta & 0 & \rho & 0 & 0 & \cdots \\ H/\beta - 1 & \rho u & \rho v & \rho & 0 & \cdots \\ Y_i/\beta & 0 & 0 & 0 & \rho & \cdots \\ \cdots & \cdots & \cdots & \cdots & \cdots & \cdots \end{bmatrix} \tag{5}$$

was applied to the pseudotime term, and the backward difference method was used. According to the Yoon and Jameson [18] lower–upper symmetric Gauss–Seidel (LU-SGS) techniques, the final form of the discretized equation, which was used to simulate the internal flow of thruster in this study, can be expressed as

$$\left\{\Gamma^{(m)} + \Delta\tau^*\left[\left(\frac{\partial}{\partial \xi}A^{(m)} - \frac{\partial}{\partial \xi}R_{\xi\xi}^{(m)}\frac{\partial}{\partial \xi}\right) + \left(\frac{\partial}{\partial \eta}B^{(m)} - \frac{\partial}{\partial \eta}R_{\eta\eta}^{(m)}\frac{\partial}{\partial \eta}\right) + D_2^{(m)}\right]\right\}\Delta\hat{Q}^{(m)} = -\Delta\tau^*(R^{(m)})^p \tag{6}$$

where

$$(R^{(m)})^p = \frac{\partial(\tilde{E}^{(m)} - \tilde{E}_v^{(m)})}{\partial \xi} + \frac{\partial(\tilde{F}^{(m)} - \tilde{F}_v^{(m)})}{\partial \eta} - \tilde{D}_{\text{ex}}^{(m)}$$

where the superscript p represents the previous iteration level, Γ is preconditioned matrix, and D_2 is the dissipation term of the second-order central difference and is efficiently eliminated by introducing D_{ex}, which consists of second- and forth-order artificial damping terms for the oscillation of the solution due to the central difference method. $\mathbf{A}^{(m)}$ and $\mathbf{B}^{(m)}$ are the inviscid term Jacobians, and $R_{\xi\xi}^{(m)}$ and $R_{\eta\eta}^{(m)}$ are the viscous term Jacobians. The scaling factor β used in the preconditioned matrix is expressed as

$$\beta = \min[a^2, \max(u^2 + v^2, U_{\text{ref}}^2)] \tag{7}$$

where U_{ref} is the reference velocity, which is greater than zero, and a denotes the velocity of sound. The solution of Eq. (6) was derived by the LU-SGS technique [18], with second-order accuracy. The turbulent effect is calculated by using the low-Reynolds-number model of Shin and Lumley [19].

B. Verification of the Numerical Scheme

The numerical scheme developed in this work was compared with the JPL nozzle test results [16]. A JPL nozzle is an axisymmetric nozzle with a 45 deg slope at the converging area and a 15 deg slope at the diverging area. A stagnation condition was applied to the entrance of the nozzle and a supersonic condition was applied to the exit of the nozzle. The temperature and pressure at the stagnation point were 300 K and 4.83 bar. The grid system consisted of 61

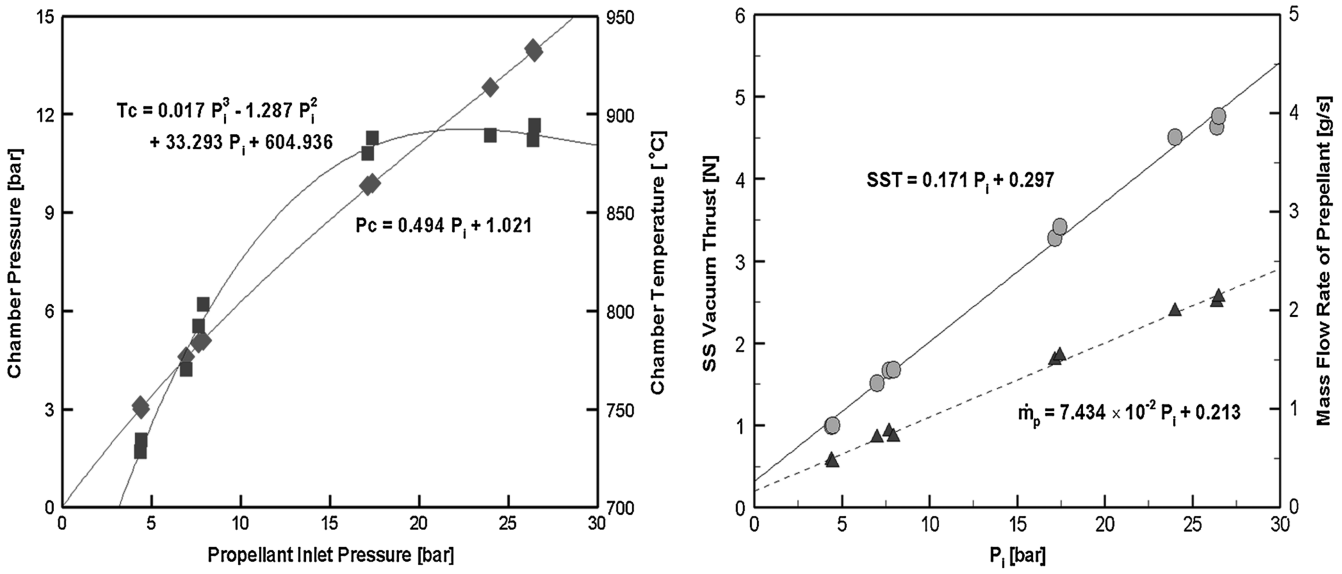

a) T_C and P_C vs P_i **b) SST and $\dot{m}_p$ vs P_i**

Fig. 4 Input data correlation from hot-fire test results.

uniform grids along the axis direction and 41 nonuniform grids along the radial direction. Figure 5 shows the JPL nozzle and the grid system employed.

Figure 6 shows the analysis results and test results [16] along the nozzle's centerline. Because of the characteristics of the converging–diverging nozzle, flow speed rapidly increased up to the supersonic range after reaching Mach 1 at the nozzle throat and the pressure decreased when the nozzle flow velocity increased. Figure 6 shows that the analysis results from the developed numerical scheme agreed well with the test results by Cuffel et al. [16].

IV. Hydrazine Thruster Performance Prediction

A. Catalytic Reaction of Hydrazine and Fraction of Ammonia Dissociation

Catalytic reactions of hydrazine with iridium are consecutive decomposition processes. These processes can be expressed as

$$3N_2H_4 \rightarrow 4NH_3 + N_2 \tag{8}$$

$$4NH_3 \rightarrow 2N_2 + 6H_2 \tag{9}$$

The hydrazine propellant is decomposed to ammonia and nitrogen by the iridium catalyst in the first chemical reaction step, which is an exothermic reaction process. The ammonia formed in the first reaction step is further dissociated to nitrogen and hydrogen in the second chemical reaction step, which is an endothermic reaction. Some of the heat generated in the first reaction step is consumed by the ammonia dissociation of the second reaction step. In the actual chemical reaction process, the first reaction step, Eq. (8), is completed as the hydrazine passes the catalyst bed. In contrast, the ammonia dissociation process, Eq. (9), is not fully completed. This means that some fraction of the ammonia formed by the first reaction step is dissociated in the second step. As a result, the consecutive reaction processes can be merged into one reaction process, which can be expressed as

$$3N_2H_4 \rightarrow 4(1-\chi)NH_3 + (1+2\chi)N_2 + 6\chi H_2 \tag{10}$$

where χ is the fraction of ammonia dissociation.

The fraction of ammonia dissociation is one of the most critical design variables. The value of χ, which is determined by the flow conditions, the composition of the catalyst, and the shape of the catalyst bed, has a range from 0 to 1. The fraction of ammonia dissociation affects the equilibrium composition of the catalytic decomposition products, the average molar mass, and the resultant temperature of the chemical reaction. These factors are important for determining the thrust and specific impulse of the monopropellant hydrazine rocket engine [12,13].

It is difficult to measure χ directly during a hot-fire test in a vacuum chamber. The test had to follow a predefined procedure, with a small hole for the measurement of the static pressure of the decomposition chamber. Basic data, such as the pressure, temperature, and the propellant mass flow rate, were obtained from the hot-fire test, but the fraction of ammonia dissociation, χ, was not available. In other words, apart from χ, we used real data for our numerical work as much as possible to produce a reliable tool for our future work.

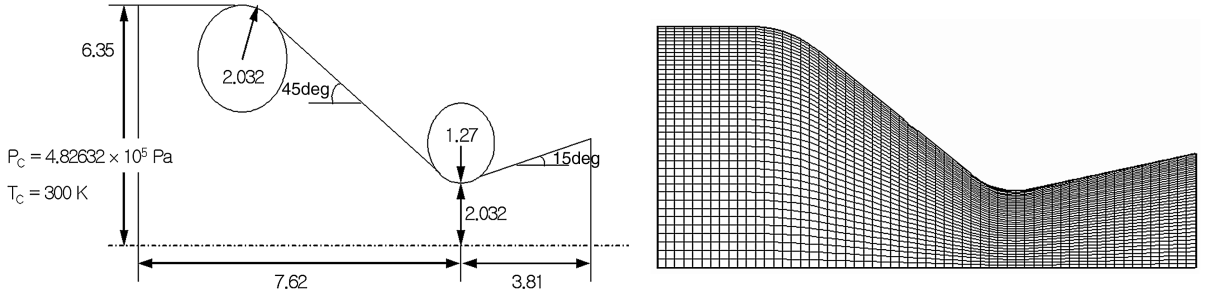

a) Geometrical shape **b) Computational grid**

Fig. 5 JPL nozzle.

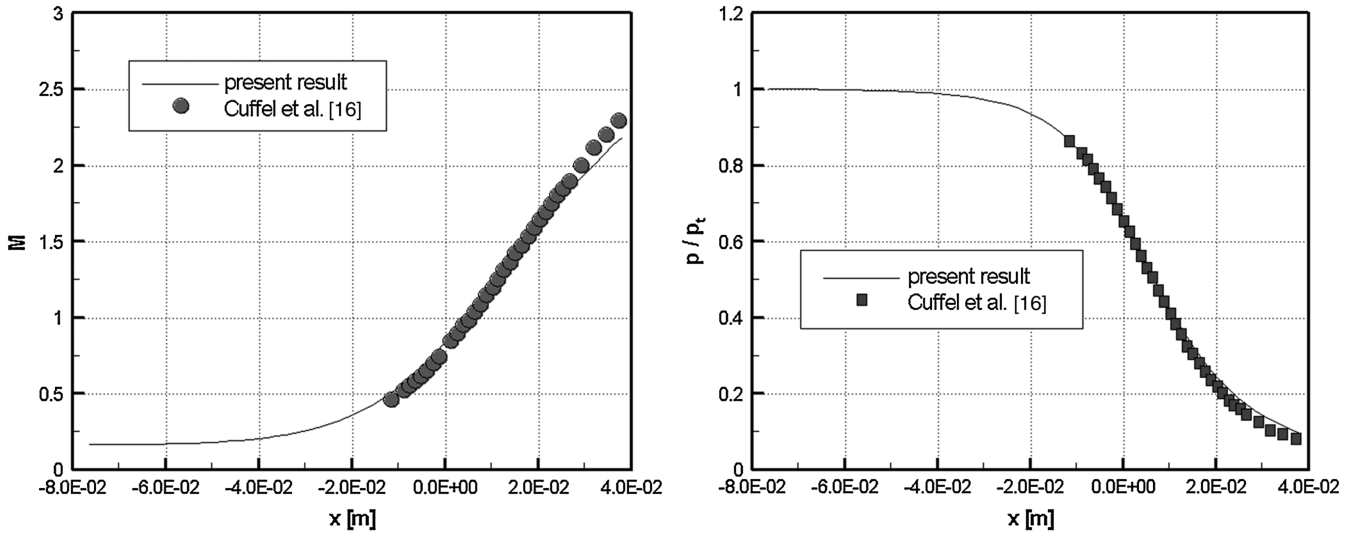

a) Mach number **b) Pressure**

Fig. 6 Numerical validation result.

The present study used the formula to predict the fraction of ammonia dissociation, which can be expressed as

$$\chi = \frac{1649 - T_C[K]}{782} \tag{11}$$

Altman et al. [20] noted that sufficient heat was liberated to heat the gases to 1649 K if N_2H_4 decomposed to NH_3 and N_2 adiabatically, which is the case for $\chi = 0$. If, however, equilibrium dissociation of NH_3 occurred, that is, $\chi = 1$, the temperature of the gases was only 867 K. They also mentioned that the dissociation of NH_3 proceeded more slowly than the N_2H_4 decomposition process from the experimental results. This fact implies the validity of assuming that the reactions cease after the gases have left the catalyst bed, thus freezing the chemical composition of the gases and fixing the performance of the thruster [11].

Legge and Dettleff [21] measured the pressure and heat transfer for three different types of thrusters, 0.5, 2, and 5 N. Their objective was to determine reliable model input values for real thrusters. Based on the characteristic of hydrazine decomposition investigated by Altman et al. [20], their test results were compared with the numerical predictions calculating the fraction of ammonia dissociation by a simple linear interpolation with a function of the temperature only, similar to Eq. (11). Numerical results using this sort of approach showed good agreement with their test output. It should be noted that their simple model to calculate χ wasn't related to any specific thrusters. On the other hand, Shankar et al. [11] acquired hot-fire test data using the 10 N Indian hydrazine thruster. They also compared those test data with their theoretical analysis results by using a one-dimensional isentropic relation. The same model to calculate the fraction of ammonia dissociation, thereby predicting the gas composition, was used, and the calculated performance of the thruster agreed well with their test data. These results imply that a simple model to calculate χ, such as Eq. (11), may induce the acceptable error for the prediction of χ and the associated performance of a hydrazine thruster. Therefore, Eq. (11) was introduced in the present study without additional verification by the test itself. Comparisons were made between test data and analysis results using Eq. (11), and they agreed well, as shown in Sec. IV.B.

B. Numerical Simulation Procedure

The temperature and pressure of the catalyst bed exit were obtained by Eqs. (1) and (2). These values were treated as the initial stagnation point conditions for a nozzle flow analysis. The mole fractions of gas species produced by the hydrazine chemical reaction flowing from the catalyst bed exit to the stagnation region of the decomposition chamber, including NH_3, N_2, and H_2, were determined by the catalyst bed temperature [20,21]. It was also assumed that the mole fractions of the injected gas species are invariant under a frozen equilibrium condition flowing through the nozzle [12,13].

The fraction of ammonia dissociation, χ, can be determined by the gas temperature of the catalyst bed, whereas the gas mole fraction, X_k, can be determined by the reaction process designated in Eq. (10). The gas mass fraction of each species, Y_k, can be determined by the following equation:

$$Y_k = \frac{X_k W_k}{\sum_{j=1}^{k} X_j W_j} \tag{12}$$

where the subscript k is the kth chemical species, and W is the molecular mass of the chemical species.

The temperature and pressure from Eqs. (1) and (2) and the gas mass fraction from Eq. (12) are assumed to be under stagnation conditions, and the supersonic boundary condition is applied at the nozzle exit. An adiabatic condition is applied along the nozzle wall. A nonuniform 121×81 grid system was applied to the nozzle's axisymmetric section after several verification simulations for grid dependency. Figure 7 shows the employed grid system.

The thrust and specific impulse could be calculated by the following equations:

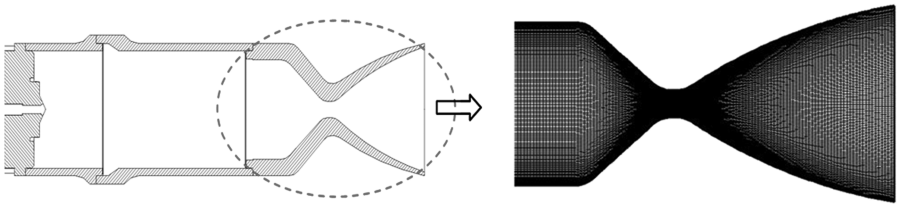

Fig. 7 Computational grid.

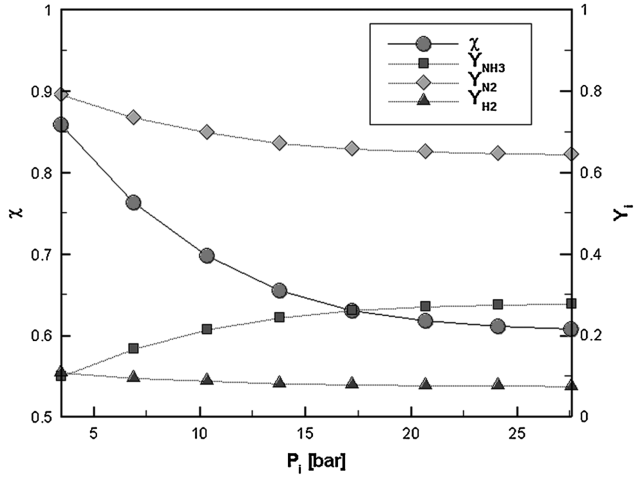

Fig. 8 Change of mass fraction with fraction of ammonia dissociation.

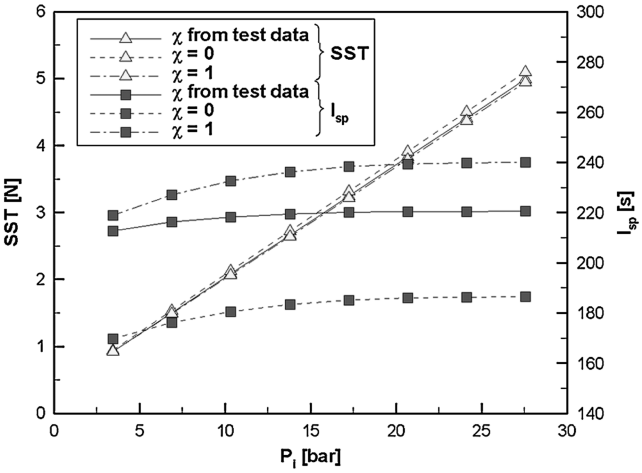

Fig. 9 Influence of fraction of ammonia dissociation on thrust and specific impulse.

$$F = \int_S \rho_e u_e^2 \, \mathrm{d}S = \int_S \dot{m}_e u_e \, \mathrm{d}S \tag{13}$$

$$I_{\mathrm{sp}} = F/\dot{m}_p g \tag{14}$$

where F denotes the thrust, and I_{sp} denotes the specific impulse. $\dot{m}_e$, ρ_e, and u_e denote the exhausted mass flow, density, and velocity at the nozzle exit, respectively, whereas g denotes the gravitational acceleration, which has a value of 9.81 m/s^2.

The thermodynamic properties of the mixed gas in the thruster are computed by Eqs. (15–17). The coefficients of these equations were obtained from Chemkin-II [22].

$$C_{pk}/R = a_{1k} + a_{2k}T + a_{3k}T^2 + a_{4k}T^3 + a_{5k}T^4 \tag{15}$$

$$\frac{H_k}{RT} = \frac{1}{RT}\int_0^T C_{pk}\,\mathrm{d}T = a_{1k} + \frac{a_{2k}}{2}T + \frac{a_{3k}}{3}T^2 + \frac{a_{4k}}{4}T^3 + \frac{a_{5k}}{5}T^4 + \frac{a_{6k}}{T} \tag{16}$$

$$\frac{S_k}{R} = \int_0^T \frac{C_{pk}}{RT}\,\mathrm{d}T = a_{1k}\ln T + a_{2k}T + \frac{a_{3k}}{2}T^2 + \frac{a_{4k}}{3}T^3 + \frac{a_{5k}}{4}T^4 + a_{7k} \tag{17}$$

where C_{pk}, H_k, and S_k are the specific heat of constant pressure, the enthalpy, and the entropy of the kth chemical species in the gas mixture, respectively; R is the universal gas constant.

The transport properties of the chemical species can be derived from Eqs. (18) and (19). The coefficients of these equations come from the data of Raznjevic [23]:

$$\mu_k = C_{\mu k}(0) + C_{\mu k}(1)T + C_{\mu k}(2)T^2 + C_{\mu k}(3)T^3 + C_{\mu k}(4)T^4 \tag{18}$$

$$k_k = C_{kk}(0) + C_{kk}(1)T + C_{kk}(2)T^2 + C_{kk}(3)T^3 + C_{kk}(4)T^4 \tag{19}$$

where μ_k and k_k are the viscosity and the conductivity of the kth species, respectively.

V. Results and Discussion

In this study, the fraction of ammonia dissociation was deduced based on the test results, whereas the composition of the gas species was obtained by the presumed fraction of ammonia dissociation. The fraction of ammonia dissociation is a critical variable for predicting the performance of a thruster. Thus, the performance variation of the thruster was first predicted for various fractions of ammonia dissociation using a theoretical one-dimensional isentropic analysis. Next, a numerical simulation was conducted to predict the

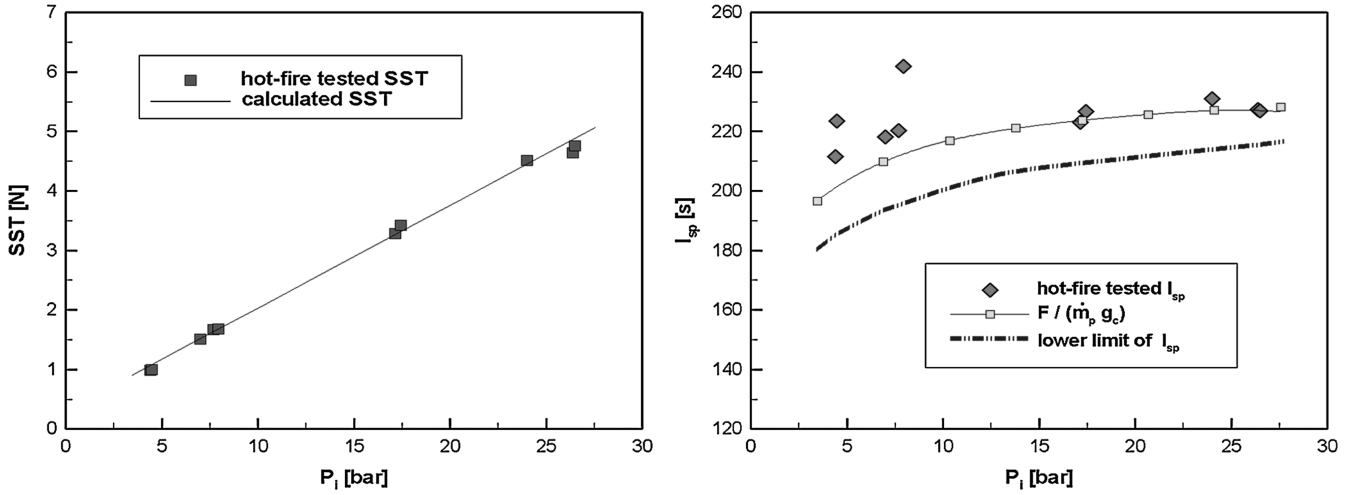

a) Steady-state thrust **b) Specific impulse**

Fig. 10 Comparison of analysis result with hot-fire test data.

Table 2 Comparison between nominal and calculated performance

	Nominal		Calculated		
P_i, bar	SST, N	I_{sp}, s	SST, N	I_{sp}, s	Error, %
24.1	4.45	-	4.47	-	0.44
3.4	0.9	-	0.9	-	0.18
21.37	-	221	-	226.06	2.29
4.48	-	202	-	201.38	0.3

performance of a KARI satellite thruster using the analysis code developed in this study. The analysis results were compared with the hot-fire test results.

A. Relation Between Fraction of Ammonia Dissociation and Thruster Performance

One of the most important variables for predicting the performance of a thruster is the mass fraction of ammonia in the gas expelled from the catalyst bed to the nozzle, which can be expressed in terms of the fraction of ammonia dissociation. The fraction of

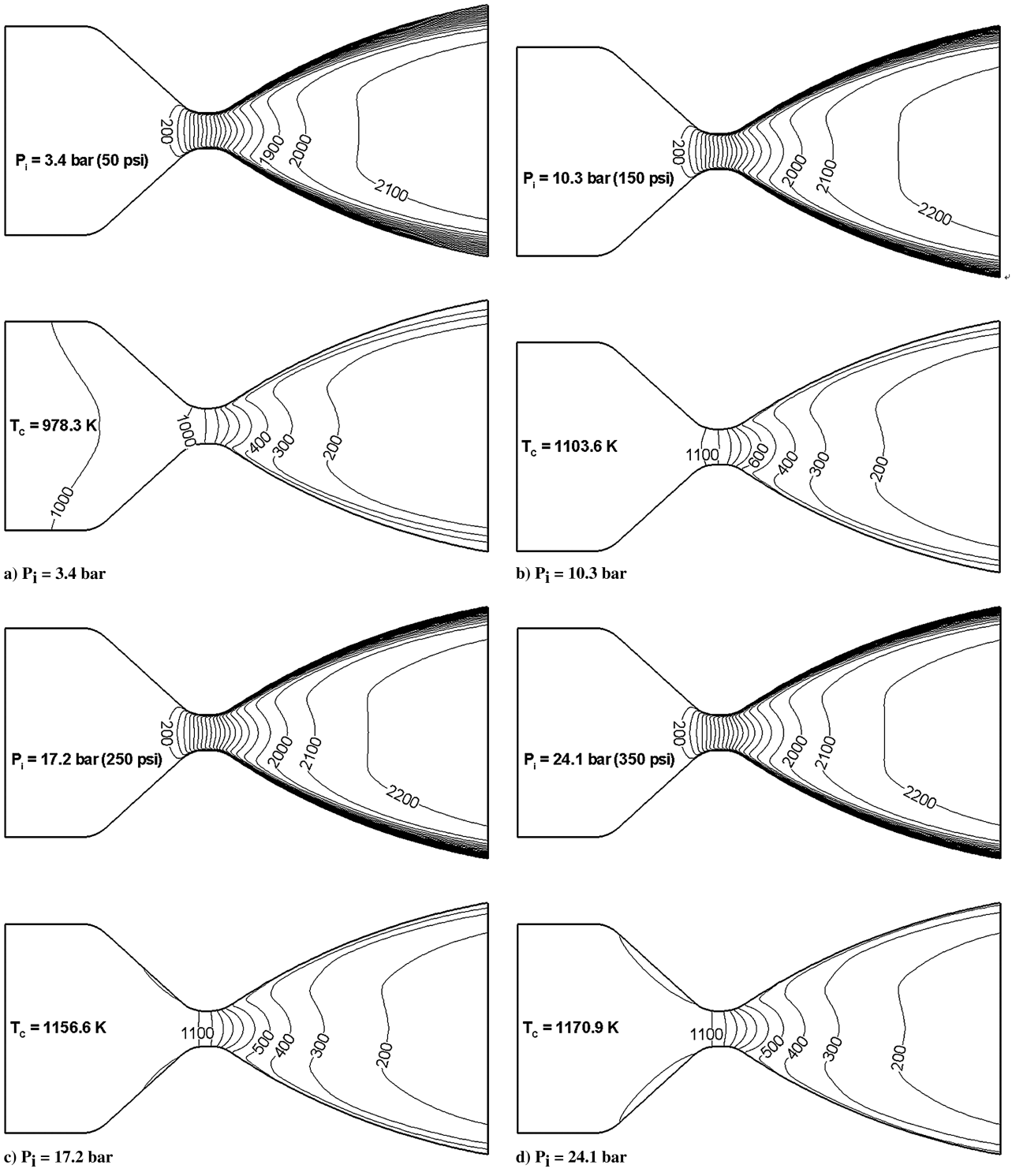

Fig. 11 Internal flow characteristics of velocity (upper) and temperature (lower) field.

ammonia dissociation cannot be found without measuring the composition of the gas mixture at the exit of the catalyst bed.

An arbitrarily assumed fraction of ammonia dissociation was used as a parameter to check the influence of the fraction of ammonia dissociation on the thruster performance using a one-dimensional isentropic flow analysis method [3]. To compare the analysis results with the test results, all variables deduced from the hot-fire test were used, that is, temperature, pressure, and propellant mass flow rate data; only the fraction of ammonia dissociation was varied.

Figure 8 shows the difference among the chemical species with variation in the fraction of ammonia dissociation. The fraction of ammonia dissociation was calculated with Eq. (11). The fraction of ammonia dissociation decreases as the propellant inlet pressure increases. The mass fraction of nitrogen increases as the fraction of ammonia dissociation decreases.

Figure 9 indicates the changes in the thrust and specific impulse at three values of the fraction of ammonia dissociation, $\chi = 0$, $\chi = 1$, and χ, from the test data ($0 < \chi < 1$). The change in the steady-state thrust as a function of the fraction of ammonia dissociation was very small; however, the change in the specific impulse was large enough so that it could not be ignored.

When the specific impulses of two extreme values of the fraction of ammonia dissociation, that is, $\chi = 1$ and $\chi = 0$, were compared, the specific impulse of $\chi = 1$ is about 29% larger than that of $\chi = 0$, irrespective of propellant inlet pressure. The theoretical specific impulse is expressed as a function of the temperature as

$$I_{sp} \propto \sqrt{T_C/M} \tag{20}$$

In practice, the theoretical specific impulse decreases as the fraction of ammonia dissociation increases because an increase in the fraction of ammonia dissociation results in a decrease in the average gas molecular mass by an increase in the hydrogen mass due to the decomposition of ammonia. It also results in a decrease in the catalyst bed outlet temperature.

The result shown in Fig. 9 was opposite that which was expected from the general relation between the specific impulse and the fraction of ammonia dissociation. It was assumed that this result was caused by the temperature at the catalyst bed exit, which is constant regardless of the fraction of ammonia dissociation. The result of such an assumption is that a change in the fraction of ammonia dissociation is only seen to cause a change in the average molecular mass of the gas. The difference in the specific impulse shown in Fig. 9 indicates that such an assumption about the fraction of ammonia dissociation is unsuitable and leads to an error when calculating the propellant budget for a satellite.

The fraction of ammonia dissociation and the composition of the chemical species in the gas mixture, which is determined by the fraction of ammonia dissociation, are important factors when analyzing the specific impulse.

B. Numerical Analysis Results

A numerical analysis of the thruster's performance was conducted and the results were verified with the test data. The propellant inlet pressure was changed from 3.45 to 24.13 bar. The fraction of ammonia dissociation used in this study was obtained from the test data.

Figure 10a shows the analysis results for the comparison between the steady-state thrust and the hot-fire test data. Overall, the analysis results for the steady-state thrust agreed well with the test data, with a 2% error tolerance. The analysis result for a specific impulse was also compared with the test data, as shown in Fig. 10b.

The predicted specific impulse agreed well with the test data for the high-inlet-pressure regime, but not for the low-inlet-pressure regime.

A turbine-type flowmeter was used to measure the flow rate during the hot-fire test and caused inaccurate flow rate measurement values in the low-inlet-pressure regime. This resulted in relatively high uncertainty of mass flow and, by extension, an increase in the dispersion of the specific impulse data, even though the thrust was measured accurately. It is assumed that a Coriolis-type flowmeter could improve the flow rate measurement accuracy. Given this uncertainty in flow measurements, it is assumed that the discordance between the model and test results in the low-inlet-pressure regime was driven by the large dispersion of the test data for the specific impulse.

Table 2 further illustrates the accuracy of the numerical solution. Results for the thrust had good accuracy compared with the nominal performance over the entire inlet pressure range.

The results summarized in Table 2 show that the calculated result for the specific impulse agreed well with the nominal specific impulse at the two extreme inlet pressures. This result suggests that the calculated specific impulses are valid even though dispersion exists in the test data.

Figure 11 shows the velocity field and temperature field inside a hydrazine thruster analyzed by the axisymmetric two-dimensional simulation programs. The results provided a spatial distribution of important variables inside a thruster, which cannot be found by one-dimensional theoretical analysis. Therefore, the results are valuable to understand the behavior of the flowfield inside a thruster.

The velocity at the centerline was faster than the velocity near the nozzle wall at the converging region before the nozzle throat; however, the velocity at the centerline was lower than the velocity near the nozzle wall at the diverging region after the nozzle throat because of the expansion of flow in the radial direction. This result indicates that the curvature of the isovelocity line changes as the flow passes the nozzle throat. The figures also show the boundary layer at the nozzle wall, which is primarily governed by turbulent effects. The centerline velocity is higher than that near the nozzle wall because flow expansion in the radial direction is almost complete in the far rear flow region after the nozzle throat.

The temperature field of the gas flow inside the thruster decreases as the flow moves to the nozzle exit due to the expansion of the gas flow. The isotherms and isovelocity line in the rear region of the nozzle throat have sharp curvatures near the nozzle wall, and these sharp curvatures also move to the nozzle exit. This means that there is a weak oblique shock wave at the sharp curvature caused by the difference in the radii of the curvatures at the junction point between the circular arc of the nozzle throat and the nozzle expansion wall. The oblique shock wave occurs as flow passes this junction point with supersonic velocity. It is also assumed that the occurrence of this oblique shock wave was driven by the fact that the centerline velocity remains supersonic until the nozzle exit.

Figure 12 shows the centerline velocity as a function of the change in the propellant inlet pressure. The figure indicates that the increase in velocity after the nozzle throat is higher when the propellant inlet pressure is larger.

Figure 13 displays the temperature and pressure distributions at the nozzle centerline and nozzle wall. The pressure drop by flow

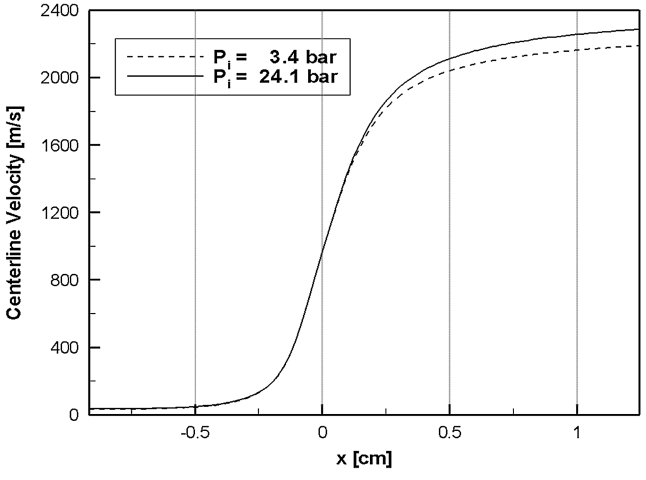

Fig. 12 Effect of propellant inlet pressure on centerline velocity.

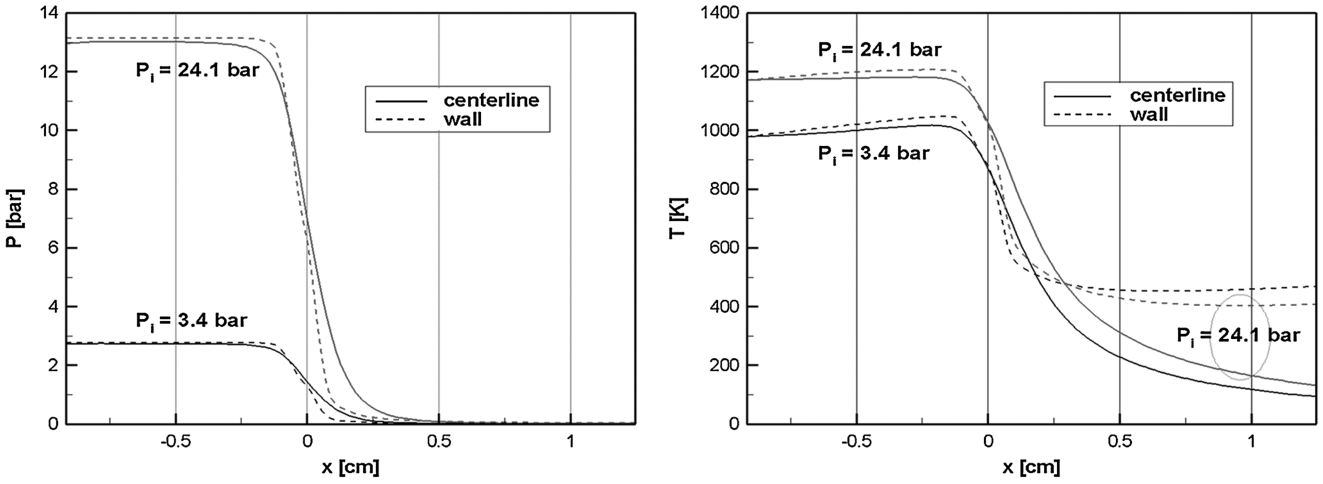

a) Pressure **b) Temperature**

Fig. 13 Variation of parameters along the nozzle wall and centerline.

acceleration at the nozzle wall is more drastic than that at the nozzle centerline just after the nozzle throat ($x = 0$) regardless of the propellant inlet pressure. The temperature variation profile has a similar behavior to the pressure drop just after the nozzle throat, with the exception of the far rear region. Temperature variation at the nozzle wall is small enough to be considered stable, however, the temperature at the nozzle centerline decreases monotonically by the continuous expansion of flow.

VI. Conclusions

The ground hot-fire test of a KARI satellite thruster was conducted under vacuum conditions. The correlation between the fraction of ammonia dissociation and thruster performance was proven using a one-dimensional isentropic analysis, and it was shown that determination of an accurate fraction of ammonia dissociation is important for predicting the thruster performance and calculating the propellant loading mass for a satellite. A reliable numerical simulation program was developed that included the concept of determining the fraction of ammonia dissociation using the catalyst bed temperature. The performance analysis results agreed well with the test data and nominal data.

The numerical program provides a two-dimensional flowfield of internal thruster operation for a wide range of propellant inlet pressures. Improved analysis results can be obtained if the adiabatic nozzle wall condition is changed to a condition that reflects the actual heat flux status of the thruster wall.

The program developed in this paper can reduce the effort needed to solve the complicated hydrazine catalytic reaction. It also reduces the analysis error caused by an arbitrary assumption of the fraction of ammonia dissociation. The analysis results are useful preliminary data for use during thruster design and are beneficial to performing precise thruster plume analyses, which require two-dimensional analysis results as input data.

References

[1] Han, C. Y., and Choi, J. M., "Thermal Analysis of Spacecraft Propulsion System and its Validation," *KSME International Journal*, Vol. 18, No. 5, 2004, pp. 847–856.

[2] Han, C. Y., Kim J. S., and Rhee, S. W., "Thermal Design for Satellite Propulsion System by Thermal Analysis," *Transactions of the Korean Society of Mechanical Engineers, B*, Vol. 27, No. 1, 2003, pp. 117–124.

[3] Brown, C. D., "Monopropellant System," *Spacecraft Propulsion*, AIAA, Washington, DC, 1995, pp. 55–63.

[4] Altman, D., and Thomas, D. D., "Evaluation of Hydrazine as Monopropellant and a Gas Generant," Jet Propulsion Laboratory, California Institute of Technology Rept. 9-36, 1949.

[5] Grant, A. F., "Development of Hydrazine as Monopropellant and Gas Generant," Jet Propulsion Laboratory, California Institute of Technology Rept. 9-1, 1950.

[6] Kersten, A. S., "Analytical Study of Catalystic Reactors for Hydrazine Decomposition," NASA United Aircraft Research Laboratories G-910461, 1968.

[7] Shankar, V., Anantha Ram, K., and Bhaskaran, K. A., "Prediction of the Concentration of Hydrazine Decomposition Products Along a Granular Catalystic Bed," *Acta Astronautica*, Vol. 11, No. 6, 1984, pp. 287–299.
doi:10.1016/0094-5765(84)90038-9

[8] Hearn, H. C., and Young, D. L., "Performance Prediction Model for a High Impulse Monopropellant Propulsion System," *Journal of Spacecraft and Rockets*, Vol. 11, No. 11, 1974, pp. 766–770.
doi:10.2514/3.27790

[9] Hearn, H. C., "Flight Performance of a High Impulse Monopropellant Thruster," *Journal of Spacecraft and Rockets*, Vol. 13, No. 5, 1976, pp. 261–265.
doi:10.2514/3.27905

[10] Subhash, G., "Empirical Simulation Model for Hydrazine Attitude Control Thrusters," *Journal of Spacecraft and Rockets*, Vol. 16, No. 6, 1979, pp. 389–393.
doi:10.2514/3.28016

[11] Shankar,V., Anantha Ram, K., and Bhaskaran, K. A., "Experimental Investigations of the 10N Catalystic Hydrazine Thruster," *Acta Astronautica*, Vol. 12, No. 4, 1985, pp. 237–249.
doi:10.1016/0094-5765(85)90038-4

[12] Adler, D., Dubrov, E., and Manheimer-Timnat, Y., "The Performance of a Hydrazine Engine with an Improved Catalyst," *Acta Astronautica*, Vol. 2, 1975, pp. 613–625.
doi:10.1016/0094-5765(75)90005-3

[13] Schmitz, B. W., and Smith, W. W., "Development of Design and Scaling Criteria for Monopropellant Hydrazine Reactors Employing Shell 405 Spontaneous Catalyst," Rocket Research Corp. Rept. 66-R-76, Vol. 2, Seattle, WA, 1967.

[14] Kushida, R., Hermel, J., Apfel, S., and Zydowicz, M., "Performance of High Area Ratio Nozzle for Small Rocket Thruster," *Journal of Propulsion and Power*, Vol. 3, No. 4, 1987, pp. 329–333.
doi:10.2514/3.22994

[15] Chen, K. H., and Shuen, J. S., "A Comprehensive Study of Numerical Algorithms for Three-Dimensional, Turbulent, Nonequilibrium Viscous Flows with Detailed Chemistry," AIAA Paper 95-0800, 1995.

[16] Cuffel, R. F., Back, L. H., and Massier, P. F., "Transonic Flowfield in a Supersonic Nozzle with Small Throat Radius of Curvature," *AIAA Journal*, Vol. 7, 1969, pp. 1968–1970.
doi:10.2514/3.5349

[17] Park, T. S., and Ryu, C. S., "Numerical Prediction of Spray Combustion and Film Cooling in a Liquid Rocket Engine," *Journal of the Korean Society of Propulsion Engineers*, Vol. 6, No. 2, 2002, pp. 9–17.

[18] Yoon, S., and Jameson, A., "An LU-SSOR Scheme for the Euler and Navier–Stokes Equations," AIAA Paper 87-600, 1987.

[19] Shin, T. H., and Lumley, J., "Kolmogorov Behavior of Near-Wall Turbulence and its Application in Turbulence Modeling," *Compressible-Fluid Dynamics*, Vol. 1, No. 1, 1993, pp. 43–56.

[20] Altman, D., Carter, J. M., Penner, S. S., and Summerfield, M., "Performance Characteristics of Monopropellant," *Liquid Propellant Rockets*, Princeton Univ. Press, 1960, pp. 92–94.

[21] Legge, H., and Dettleff, G., "Pitot Pressure and Heat Transfer Measurements in Hydrazine Thruster Plumes," *Journal of Spacecraft and Rockets*, Vol. 23, No. 4, 1986, pp. 357–362. doi:10.2514/3.25812

[22] Kee, R. J., Rupley, F. M., and Miller, J. A., "Chemkin-II: A Fortran Chemical Kinetics Package for the Analysis of the Gas Phase Chemical Kinetics," Sandia National Laboratories SAND89-8009B UC-706, Livermore, CA, 1994.

[23] Raznjevic, K., *Handbook of Thermodynamic Tables and Charts*, Hemisphere, New York/Washington, D.C., 1976.

T. Lin
Associate Editor